Available online at www.sciencedirect.com

ScienceDirect

Geochimica et Cosmochimica Acta 164 (2015) 386–402

Geochimica et Cosmochimica Acta

www.elsevier.com/locate/gca

Geodynamic controls on the contamination of Cenozoic arc magmas in the southern Central Andes: Insights from the O and Hf isotopic composition of zircon

Rosemary E. Jones [a,*], Linda A. Kirstein [a], Simone A. Kasemann [b], Bruno Dhuime [c], Tim Elliott [c], Vanesa D. Litvak [d], Ricardo Alonso [e], Richard Hinton [a], Edinburgh Ion Microprobe Facility (EIMF) [a]

[a] School of GeoSciences, University of Edinburgh, West Mains Road, Edinburgh EH9 3JW, UK
[b] Department of Geosciences & MARUM, Centre for Marine Environmental Sciences, University of Bremen, 28334 Bremen, Germany
[c] School of Earth Sciences, University of Bristol, Wills Memorial Building, Queen's Road, Bristol BS8 1RJ, UK
[d] Instituto de Estudios Andinos Don Pablo Groeber, Departamento de Ciencias Geológicas, Universidad de Buenos Aires, CONICET, Argentina
[e] Departamento de Geología, Universidad Nacíonal de Salta, CONICET, 4400 Salta, Argentina

Received 2 September 2014; accepted in revised form 5 May 2015; available online 16 May 2015

Abstract

Subduction zones, such as the Andean convergent margin of South America, are sites of active continental growth and crustal recycling. The composition of arc magmas, and therefore new continental crust, reflects variable contributions from mantle, crustal and subducted reservoirs. Temporal (Ma) and spatial (km) variations in these contributions to southern Central Andean arc magmas are investigated in relation to the changing plate geometry and geodynamic setting of the southern Central Andes (28–32° S) during the Cenozoic. The *in-situ* analysis of O and Hf isotopes in zircon, from both intrusive (granitoids) and extrusive (basaltic andesites to rhyolites) Late Cretaceous – Late Miocene arc magmatic rocks, combined with high resolution U–Pb dating, demonstrates distinct across-arc variations. Mantle-like $\delta^{18}O_{(zircon)}$ values (+5.4‰ to +5.7‰ (±0.4 (2σ))) and juvenile initial $\varepsilon Hf_{(zircon)}$ values (+8.3 (±0.8 (2σ)) to +10.0 (±0.9 (2σ))), combined with a lack of zircon inheritance suggests that the Late Cretaceous (~73 Ma) to Eocene (~39 Ma) granitoids emplaced in the Principal Cordillera of Chile formed from mantle-derived melts with very limited interaction with continental crustal material, therefore representing a sustained period of upper crustal growth. Late Eocene (~36 Ma) to Early Miocene (~17 Ma) volcanic arc rocks present in the Frontal Cordillera have 'mantle-like' $\delta^{18}O_{(zircon)}$ values (+4.8‰ (±0.2 (2σ) to +5.8‰ (±0.5 (2σ))), but less radiogenic initial $\varepsilon Hf_{(zircon)}$ values (+1.0 (±1.1 (2σ)) to +4.0 (±0.6 (2σ))) providing evidence for mixing of mantle-derived melts with the Late Paleozoic – Early Mesozoic basement (up to ~20%). The assimilation of both Late Paleozoic – Early Mesozoic Andean crust and a Grenville-aged basement is required to produce the higher than 'mantle-like' $\delta^{18}O_{(zircon)}$ values (+5.5‰ (±0.6 (2σ) to +7.2‰ (±0.4 (2σ))) and unradiogenic, initial $\varepsilon Hf_{(zircon)}$ values (−3.9 (±1.0 (2σ)) to +1.6 (±4.4 (2σ))), obtained for the Late Oligocene (~23 Ma) to Late Miocene (~9 Ma) magmatic rocks located in the Argentinean Precordillera, and the Late Miocene (~6 Ma) volcanic rocks present in the Frontal Cordillera. The observed isotopic variability demonstrates that the assimilation of pre-existing continental crust, which varies in both age and composition over the Andean Cordillera, plays a dominant role in modifying the isotopic composition of Late Eocene

* Corresponding author.
E-mail address: Rosie.Jones@earth.ox.ac.uk (R.E. Jones).

http://dx.doi.org/10.1016/j.gca.2015.05.007
0016-7037/

to Late Miocene mantle-derived magmas, implying significant crustal recycling. The interaction of arc magmas with distinct basement terranes is controlled by the migration of the magmatic arc due to the changing geodynamic setting, as well as by the tectonic shortening and thickening of the Central Andean crust over the latter part of the Cenozoic.

1. INTRODUCTION

Arc magmas, and hence new crust, potentially contain components derived from a number of different reservoirs (e.g., the mantle, subducted sediments, the subducting oceanic lithosphere, continental crust from subduction erosion, and the overlying crust). The proportions of these various contributions must be investigated and determined in order to quantify net crustal growth and the long-term recycling of crustal material. Resolving mantle and subduction components is more straight-forward in oceanic arcs than continental arcs because there is limited interaction with existing continental crust (e.g., Gill, 1981). The task is more challenging for arcs built on continental crust as the addition of subducting components is notoriously difficult to resolve from the contamination of magmas with the overlying crust (e.g., Davidson et al., 1991). However, as continental margins are considered the principal site for the growth of the continental crust, determining these contributions is key to understanding the generation, evolution and reworking of continental crust over time.

The Central Andes represents a type example of an ocean–continent convergent margin and is an active site of modern continental growth. Previous studies have identified an increased influence of crustal components on arc magmas from the southern Central Andes over the course of the Cenozoic on the basis of whole rock major and trace element geochemistry, and isotopic compositions (e.g., Kay et al., 1991; Kay and Abbruzzi, 1996; Litvak et al., 2007; Goss et al., 2013). However, discriminating between the processes involved (i.e., contamination of the mantle wedge with subducted components and/or crustal material from subduction erosion, versus arc magmas assimilating existing continental crust en route to the surface) remains unresolved.

The geodynamic setting of the Central Andean margin, specifically plate convergence rates and the angle of the subducting oceanic plate, as well as the thickness of the Central Andean continental crust, has changed significantly over the course of the Cenozoic (e.g., Pilger, 1981, 1984; Pardo Casas and Molnar, 1987; Kay et al., 1991, 2005; Somoza, 1998; Yañez et al., 2001, 2002; Somoza and Ghidella, 2012; Goss et al., 2013). The Andean margin has also experienced high levels ($50\ km^3/km/Myr$ (Stern, 2011)) of subduction erosion (Rutland, 1971; Stern, 1991) and variable sediment flux from the oceans and continents (Von Huene and Scholl, 1991a). This study utilises the isotopic composition of the robust accessory mineral zircon to investigate how the changing geodynamic setting, crustal thickness, sediment flux and levels of subduction erosion along the southern Central Andean margin has affected the contamination of southern Central Andean arc magmas, and thus the extent of crustal recycling over time.

2. GEODYNAMIC AND GEOLOGICAL SETTING

Subduction has been active along the western margin of South America since the earliest Jurassic, with subduction-related magmatism in the Central Andes initiated at ~185 Ma (e.g., Pichowiak et al., 1990; Stern, 2004). The study area is located within the Pampean (Chilean) flat-slab segment (~28°–33° S) of the southern Central Andes (Fig. 1). This segment of the Andean margin has been volcanically inactive since the Late Miocene (~6 Ma) (e.g., Kay et al., 1999; Bissig et al., 2003; Litvak et al., 2007) due to a decrease in the angle (<10° at 100 km depth) at which the oceanic Nazca plate subducts beneath the South American continent (e.g., Pilger, 1981, 1984; Yañez et al., 2001). The present day, low angle of subduction has been attributed to the subduction of the Juan Fernandez Ridge (JFR) which began intersecting the Andean margin during the early Miocene (~18 Ma) (e.g., Yañez et al., 2001; Jones et al., 2014). The shallowing of the Nazca plate caused the position of the volcanic arc to expand and migrate to the east (e.g., Kay et al., 1987; Kay and Mpodozis, 2002). Convergence rates and the relative plate motions between the oceanic (Farallon and Nazca) and South American plates have also changed during the course of the Cenozoic; in particular a major plate reconfiguration occurred in the Late Oligocene (~25 Ma) due to the break-up of the Farallon plate into the Nazca and Cocos plates (Lonsdale, 2005). This resulted in an increase in convergence rates (from ~8 cm/yr to ~15 cm/yr) between the Nazca and South American plates and a change from oblique (NE–SW) to orthogonal (ENE–WSW) convergence (Pardo Casas and Molnar, 1987; Somoza, 1998; Somoza and Ghidella, 2012). This increased convergence, combined with increased compression related to the subduction of the JFR, led to an increase in crustal thickness in the southern Central Andes from ~30 km to >45 km (Kay et al., 1991; Haschke et al., 2002).

The Andean tectonic cycle (Jurassic to recent) represents only the latest in a series of orogenic cycles to affect the western edge of the South American continent. Earlier tectonic cycles (e.g., the Gondwanan tectonic cycle, latest Devonian to early Permian) along with episodes of extension, subduction and accretion formed the distinctive basement on which the modern Andes are built (Ramos et al., 1986; Charrier et al., 2007). In the Pampean flat-slab segment, the Andean margin is divided from west to east into

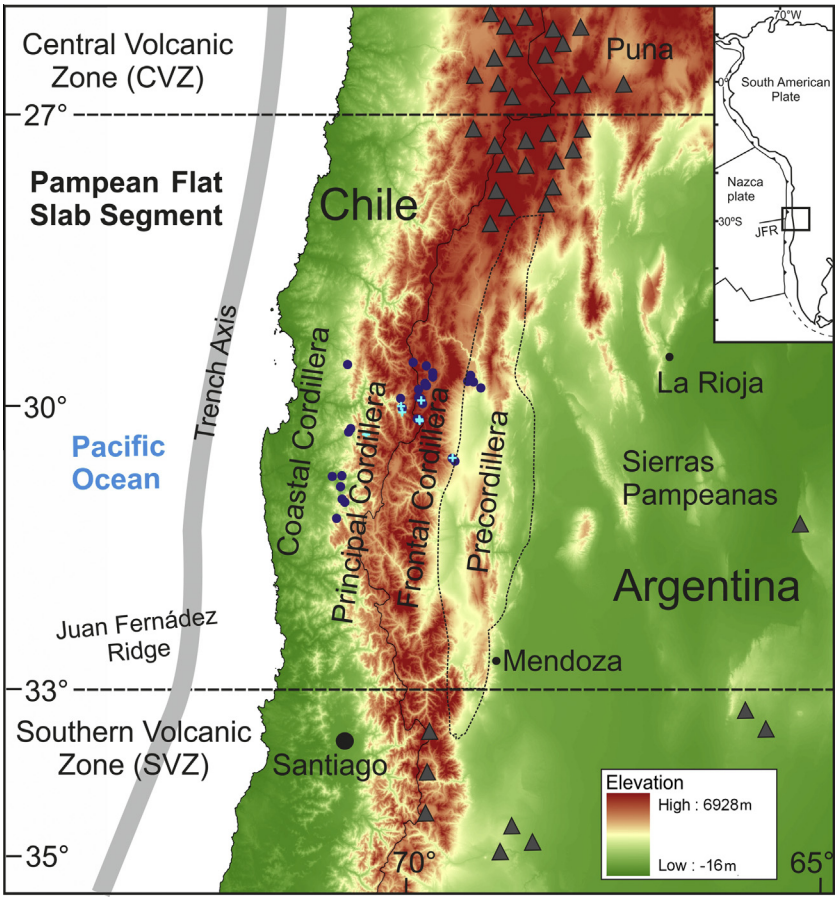

Fig. 1. Map showing the main features of the southern Central Andean margin. Sample locations are highlighted (Late Cretaceous – Miocene samples by dark blue circles and Permian – Triassic basement samples by light blue crosses) alongside the locations of the Principal Cordillera, Frontal Cordillera and Precordillera (the extent of the Precordillera terrane is outlined). Digital elevation data from Jarvis et al. (2008). Current active volcanic centres are indicated with grey triangles. (For interpretation of the references to colour in this figure legend, the reader is referred to the web version of this article.)

the Coastal Cordillera, the Principal Cordillera, the Frontal Cordillera, the Precordillera and the Sierras Pampeanas (Fig. 1). The age and origin of the underlying basement varies across the Andean Cordillera depending on the extent of these north–south trending morphostructural units. The basement of the Principal and Frontal Cordillera is composed of highly deformed Paleozoic sediments which have been intruded and covered by extensive Late Palaeozoic – Early Mesozoic plutons and volcanic rocks (Kay et al., 1989). In the Argentinean Precordillera (Fig. 1) a Grenville-aged basement (1200–1000 Ma), which is not exposed at the surface and has been identified through various geochemical studies, is overlain by Cambrian – Ordovician strata (Kay and Abbruzzi, 1996; Kay et al., 1996; Thomas et al., 2004; Ramos, 2010). As a result of both the regional geology and the migration of the volcanic arc to the east there is a unique opportunity for a distinctive spatial relationship in the contamination of mantle-derived magmas, via assimilation and crustal reworking en route to the surface, to be revealed.

3. INSIGHTS FROM THE ISOTOPIC COMPOSITION OF ZIRCON

In continental arcs, the relative contributions to arc magmas, from mantle, crustal and subducted components can be difficult to constrain from whole rock geochemistry alone as it often reflects a complex history of fractional crystallisation and late stage alteration (e.g., McCarthy and Hasty, 1976; Marfil and Maiza, 2012). This is a particular problem in the southern Central Andes where some of the arc magmatic rocks (e.g., the Tilito Formation) have been affected by hydrothermal alteration (Bissig et al., 2001, 2003; Kay and Mpodozis, 2001; Charchaflié et al., 2007; Litvak et al., 2007). A solution is to conduct high resolution, *in-situ* oxygen and hafnium isotopic analysis of the robust accessory mineral zircon and combine this with high resolution U–Pb dating and detailed cathodoluminescence imaging. Zircon grains also potentially preserve information about the nature of the contaminant (e.g., through the presence of xenocrystic cores), which are not apparent

from whole rock geochemistry. The analysis of individual zircon grains, which unlike whole rocks can be readily dated and reliably analysed for $\delta^{18}O$ (robust to recent alteration), by *in-situ* techniques, enables a much more detailed picture of the relative contributions to arc magmas to be achieved.

Specifically, the combination of oxygen and hafnium isotopic variations in zircon can be used to investigate the interactions between mantle-derived melts and older crustal material (e.g., Hawkesworth and Kemp, 2006; Kemp et al., 2007). Assuming zircon crystallisation is cogenetic (i.e., the zircon has not been inherited from elsewhere), zircon will retain the oxygen isotope composition of the melt from the time of crystallisation (Peck et al., 2003). Zircons which crystallise in equilibrium with melts derived from an uncontaminated mantle source have a narrow range of $\delta^{18}O$ values ($5.3 \pm 0.6‰$ (Valley et al., 1998; Valley, 2003)). As oxygen isotopes are sensitive to water–rock interactions and the fractionation of oxygen isotopes increases with decreasing temperature (Clayton et al., 1972), the interaction of magmas with sediments and/or low temperature altered crust leads to elevated $\delta^{18}O_{(zircon)}$ values. Thus, higher than 'mantle like' $\delta^{18}O_{(zircon)}$ values suggests the incorporation of a ^{18}O enriched supracrustal component, such as sediment, into the magma from which the zircon crystallised (e.g., Eiler, 2001).

Hafnium (Hf) is more incompatible than lutetium (Lu) during the melting of spinel and garnet peridotite. Thus crust is formed with low Lu/Hf and with time the radioactive decay of ^{176}Lu to ^{176}Hf results in the crust evolving with a less radiogenic $^{176}Hf/^{177}Hf$ composition relative to the mantle from which it separated (Patchett et al., 1982; Kinny and Maas, 2003). Therefore, the mixing of new mantle-derived melts with older, and hence less radiogenic crust (e.g., a Grenville-aged basement), will lead to lower epsilon Hf values (i.e., the $^{176}Hf/^{177}Hf$ expressed in parts per ten thousand difference relative to a chondritic reservoir) in the zircon crystallising from the magma. In addition to this, where there is no evidence for mixing with older crustal material (i.e., high initial $\varepsilon Hf_{(zircon)}$ values, 'mantle-like' $\delta^{18}O_{(zircon)}$ values and no zircon inheritance) Hf model ages can be used to identify when a primary melt differentiated from the primitive mantle (e.g., Hawkesworth and Kemp, 2006). Combining zircon U–Pb crystallisation ages with Hf model ages therefore has the potential to reveal periods of new crustal growth (e.g., Belousova et al., 2010; Dhuime et al., 2011).

We have applied these techniques to zircons separated from representative samples of both intrusive (diorites to granites) and extrusive (basaltic andesites to rhyolites) Late Cretaceous – Late Miocene arc rocks. These samples were collected from an W–E transect across the Andean Cordillera from Chile into Argentina, between 29 and 31° S (Fig. 1 and Table 1). All the major plutonic and volcanic formations, which had previously been mapped as between Late Cretaceous – Late Miocene in age (Maksaev et al., 1984; Mpodozis and Cornejo, 1988; Nasi et al., 1990; Cardó and Díaz, 1999; Emparan and Pineda, 1999; José Frutos et al., 2004; Pineda and Emparan, 2006; Cardó et al., 2007; Pineda and Calderón, 2008), were sampled from this region. The arc rocks sampled from the Principal Cordillera of Chile, which are primarily plutonic and belong to the Cogotí Supergroup, range in age from the Late Cretaceous (72.6 ± 0.8 Ma) to the Eocene (38.9 ± 1.0 Ma), as determined by the U–Pb dating conducted as part of this study (Table 1). The samples collected from the Frontal Cordillera range in age from the Early Paleocene (61.9 ± 9.1 Ma) to the Late Miocene (6.2 ± 0.3 Ma) and are primarily extrusive, and the plutonic and volcanic rock samples collected from the Precordillera of Argentina (i.e., furthest east) range in age from the Late Oligocene (22.6 ± 0.3 Ma) to the Late Miocene (9.4 ± 0.2 Ma) (Table 1). Zircons were also separated from a number of plutonic and volcanic rocks from the Late Palaeozoic – Early Mesozoic basement, which were collected in order to characterise potential contaminants of the Late Cretaceous – Late Miocene arc magmas. These samples range in age from 280.2 ± 3.5 Ma to 221.0 ± 4.4 Ma (Table 1).

Detailed petrographic analysis and cathodoluminescence imaging (Fig. 2) of individual zircon grains was conducted in order to identify the magmatic origin of the zircon grains, and suitable grains and specific locations for isotopic analysis (refer to Section 2 of the Appendix). This included the identification of magmatic zircon grains with simple histories and those with distinct xenocrystic cores which may reveal the nature and age of the contaminating crustal material (Fig. 2). Oxygen isotope compositions and U–Pb crystallisation ages were determined from the same zircon growth zones using a Cameca ims 1270 secondary ion mass spectrometer (SIMS) at the NERC Ion Microprobe Facility, University of Edinburgh (Fig. 2 and Appendix). Subsequently, hafnium isotope analysis was conducted on a multi-collector inductively-coupled plasma mass spectrometer combined with a laser ablation system (LA-MC-ICPMS), at the University of Bristol. Full details of analytical methods and data correction are presented in the Appendix.

4. RESULTS

Sample summary information is presented in Table 1. Full results are presented in Figs. 3 and 4, and Table A1 and A2 of the Appendix.

4.1. Oxygen isotopes

No correlation is apparent between the $\delta^{18}O_{(zircon)}$ values and the whole rock SiO_2 content as shown in Fig. 3a. The $\delta^{18}O$ values obtained for individual zircon grains from the Late Cretaceous (72.6 Ma) to Eocene (38.9 Ma) plutonic rocks located in the Principal Cordillera of Chile, range between 4.96‰ (±0.33 (2σ)) and 6.13‰ (±0.33 (2σ)) (Fig. 4). These values are all within analytical uncertainty of those expected for zircon crystallising in isotopic equilibrium with mantle-derived melts ($5.3‰ \pm 0.6$ (Valley et al., 1998)). With the exception of the most easterly sample of the Tilito Formation (PC14), the majority of $\delta^{18}O_{(zircon)}$ values obtained for the Early Paleocene (61.9 Ma) to Late Miocene (6.2 Ma) arc rocks located in

Table 1
Summary sample information. The reported U–Pb ages (Ma) are sample ages as given by Concordia diagrams and Terra-Wasserberg plots (Jones, 2014). The whole rock major element compositions were determined by X-ray florescence spectrometry (XRF). Whole rock data for sample DI095 is from Litvak et al. (2007).

Sample	Latitude (S)	Longitude (W)	Cordillera	Geological Group/ Formation/Unit	Rock type	SiO_2 (wt%)	TiO_2 (wt%)	Al_2O_3 (wt%)	Fe_2O_3 (wt%)	MnO (wt%)	MgO (wt%)	CaO (wt%)	Na_2O (wt%)	K_2O (wt%)	P_2O_5 (wt%)	U-Pb age (Ma)	$\pm 2\sigma$ or 95% conf.
RJ11A18	−30.55025	−69.46478	Precordillera	Pluton Tocota (Colangüil Batholith)	Granodiorite	68.69	0.59	15.07	3.91	0.08	1.55	2.91	3.52	3.15	0.18	280.2	3.5
MQ39	−29.98694	−69.81694	Frontal Cordillera	Choiyoi Group	Rhyolite	73.70	0.31	13.92	1.69	0.05	0.25	0.52	3.44	5.70	0.04	269.7	2.6
RJ11A20	−30.20286	−69.82981	Frontal Cordillera	Choiyoi Group	Rhyolite	74.72	0.24	13.87	1.35	0.03	0.19	0.43	3.49	5.51	0.02	269.6	7.0
AM0862	−30.16139	−69.86500	Frontal Cordillera	Choiyoi Group	Rhyolite	73.88	0.33	14.37	1.61	0.05	0.22	0.14	3.48	5.39	0.03	269.3	5.2
AM0853	−30.20482	−70.04247	Frontal Cordillera	Pastos Blancos Group	Rhyolite											261.0	6.0
AM0855	−30.12487	−70.06505	Frontal Cordillera	Pastos Blancos Group	Rhyolite											248.6	5.5
RJ1104	−30.23869	−70.34286	Principal Cordillera	El León Unit (Ingaguás Supergroup)	Granite	76.74	0.14	12.99	1.13	0.04	0.24	0.66	3.77	3.98	0.02	221.0	4.4
AM0812	−30.74000	−70.86083	Principal Cordillera	Cogotí Supergroup	Diorite	61.06	0.72	16.70	6.52	0.13	2.76	5.75	3.48	2.19	0.15	72.55	0.77
AM0823	−30.98639	−70.74083	Principal Cordillera	Cogotí Supergroup	Granodiorite	65.16	0.56	16.88	1.78	0.04	1.96	4.50	7.96	0.50	0.14	69.80	0.73
AM0824	−30.98639	−70.74083	Principal Cordillera	Cogotí Supergroup	Syeno-diorite	60.27	0.82	17.50	6.61	0.15	2.38	5.23	4.39	2.38	0.18	64.59	0.65
AM0806	−30.73500	−70.75861	Principal Cordillera	Cogotí Supergroup	Granite	68.75	0.46	15.20	3.37	0.07	0.87	2.27	3.86	4.76	0.08	64.39	0.66
RJ1103	−31.00108	−70.72181	Principal Cordillera	Cogotí Supergroup	Syeno-diorite	61.93	0.75	17.09	5.97	0.11	2.06	4.71	4.58	2.43	0.18	64.33	0.59
AM0826	−30.98639	−70.74083	Principal Cordillera	Cogotí Supergroup	Granite	66.94	0.56	15.68	4.01	0.03	1.29	2.73	4.22	4.16	0.10	64.21	0.69
AM0890	−29.94444	−70.07111	Frontal Cordillera	Los Elquinos Formation	Basaltic andesite	55.44	1.12	18.46	8.53	0.14	3.74	6.84	3.03	1.92	0.44	62.00	38.00
AM0822	−30.25250	−70.65028	Principal Cordillera	Cogotí Supergroup	Granodiorite	66.58	0.42	16.83	3.95	0.16	1.05	3.34	5.22	2.19	0.19	57.30	1.70
AM0815	−30.84111	−70.77167	Principal Cordillera	Cogotí Supergroup	Granodiorite	67.37	0.43	15.85	3.94	0.08	1.63	3.75	3.94	2.61	0.11	55.00	1.70
AM0816	−30.84111	−70.77167	Principal Cordillera	Cogotí Supergroup	Granodiorite	67.21	0.40	15.89	3.69	0.07	1.51	3.72	3.94	2.63	0.10	54.06	0.76
RJ1105	−29.59417	−70.69061	Principal Cordillera	Tierras Blancas Caldera	Diorite	58.40	0.60	18.25	6.64	0.17	4.02	6.62	3.93	1.13	0.16	40.20	1.20

RJ1101	−31.16878	−70.81919	Principal Cordillera	Cogotí Supergroup	Granite	71.32	0.24	15.15	2.53	0.06	0.98	2.99	3.80	2.60	0.09	38.89	0.99
AM0867	−30.15667	−69.87972	Frontal Cordillera	Bocatoma Unit	Andesite	58.46	0.75	19.07	6.21	0.13	2.50	6.96	3.86	1.76	0.22	35.58	0.78
AM0846	−30.04278	−70.05417	Frontal Cordillera	Tilito Formation (Lower Doña Ana Group)	Rhyolite	72.34	0.33	14.79	2.39	0.09	0.51	1.34	4.16	3.64	0.09	26.10	1.60
MQ153	−29.85272	−69.86294	Frontal Cordillera	Tilito Formation (Lower Doña Ana Group)	Andesite											25.20	0.26
AM0845	−30.04278	−70.05417	Frontal Cordillera	Tilito Formation (Lower Doña Ana Group)	Rhyolite											24.90	0.32
AM0860	−30.16139	−69.86500	Frontal Cordillera	Tilito Formation (Lower Doña Ana Group)	Dacite											24.86	0.40
ZN122	−29.57619	−69.92303	Frontal Cordillera	Tilito Formation (Lower Doña Ana Group)	Andesite	62.35	0.71	16.10	6.60	0.13	3.18	6.02	2.47	2.03	0.25	24.78	0.37
AM0844	−30.04250	−70.05194	Frontal Cordillera	Tilito Formation (Lower Doña Ana Group)	Rhyolite	74.70	0.23	13.58	1.54	0.06	0.20	0.75	4.51	3.87	0.06	24.72	0.28
AM0849	−30.04278	−70.05417	Frontal Cordillera	Tilito Formation (Lower Doña Ana Group)	Rhyolite											24.69	0.43
RF64	−29.79425	−69.77597	Frontal Cordillera	Tilito Formation (Lower Doña Ana Group)	Rhyolite											24.26	0.70
PC14	−29.44883	−69.49070	Frontal/ Precordillera	Tilito Formation (Lower Doña Ana Group)	Rhyolite	74.24	0.14	13.55	2.07	0.21	0.33	4.75	0.19	4.61	0.05	23.61	0.21
Z27	−29.61389	−69.77611	Frontal Cordillera	Tilito Formation (Lower Doña Ana Group)	Dacite	67.52	0.74	15.96	4.68	0.03	0.24	3.02	3.65	3.94	0.16	23.18	0.30
RJ11A5	−29.83542	−69.13511	Precordillera	Las Trancas Formation	Rhyolite											22.55	0.33
RJ11A10	−29.76408	−69.28128	Precordillera	Miocene Intrusives	Granite	71.14	0.23	14.92	2.64	0.06	0.43	1.88	3.81	4.14	0.10	22.17	0.23
RJ11A11	−29.71292	−69.25514	Precordillera	Miocene Intrusives	Granite	68.98	0.49	14.83	3.75	0.07	0.96	2.09	2.88	5.32	0.16	21.37	0.29
RJ11A14	−29.77164	−69.22322	Precordillera	Miocene Intrusives	Granodiorite	65.02	0.61	16.16	4.70	0.08	2.08	3.97	3.35	3.76	0.23	20.43	0.31
1026	−29.69056	−69.69500	Frontal Cordillera	Escabroso Formation (Upper Doña Ana Group)	Andesite-Trachyandesite	61.77	0.80	16.61	5.97	0.09	2.27	5.25	3.76	2.99	0.18	18.21	0.28

SP80	−29.72392	−69.69964	Frontal Cordillera	Escabroso Formation (Upper Dona Ana Group)	Andesite	60.89	0.84	16.68	6.39	0.11	2.63	5.91	3.46	2.82	0.18	18.06	0.37	
RF62	−29.79403	−69.78217	Frontal Cordillera	Cerro de las Tórtolas Formation	Trachyandesite	60.54	0.90	18.01	6.18	0.06	1.29	5.59	3.83	2.99	0.23	17.06	0.63	
RJ11A7	−30.68222	−69.43619	Precordillera	Tertiary Intrusives	Trachyandesite	63.11	0.62	16.81	4.36	0.07	2.34	4.64	5.13	2.40	0.23	11.65	0.21	
RJ11A17	−30.55664	−69.46964	Precordillera	Tertiary Intrusives	Dacite	64.39	0.60	17.24	3.96	0.07	1.47	4.79	4.83	2.04	0.24	9.45	0.18	
RJ11A15	−30.55139	−69.46786	Precordillera	Tertiary Intrusives	Trachydacite	63.85	0.64	17.18	4.16	0.07	1.62	4.52	5.13	2.16	0.26	9.43	0.18	
MQ33	−29.95314	−69.83447	Frontal Cordillera	Vacas Heladas Ignimbrites	Rhyolite	71.46	0.24	15.71	1.55	0.04	0.31	1.88	4.62	3.63	0.06	6.16	0.19	
DI095	−29.98889	−69.81833	Frontal Cordillera	Vacas Heladas Ignimbrites	Rhyolite	70.84	0.17	15.67	1.46	0.00	0.46	2.48	5.04	3.84	0.03	6.15	0.30	

the Frontal Cordillera, also lie within analytical uncertainty of 'mantle-like' values. Oxygen isotope values obtained for individual zircon grains from these primarily extrusive rocks, range between 4.57‰ (±0.27 (2σ)) and 6.47‰ (±0.27 (2σ)), displaying more variation than the plutonic samples from the Principal Cordillera (Fig. 4). The Late Oligocene (22.6 Ma) to Late Miocene (9.4 Ma) intrusive and extrusive arc rocks located in the Precordillera, along with the most easterly sample of the Tilito Formation (PC14, 23.6 Ma), have higher than 'mantle-like' $\delta^{18}O_{(zircon)}$ values, with values ranging from 5.57‰ (±0.29 (2σ)) to 7.92‰ (±0.22 (2σ)) (Fig. 4). Analysis of zircons obtained from plutonic and volcanic rocks comprising the Late Palaeozoic to Early Mesozoic basement produced varied $\delta^{18}O_{(zircon)}$ values ranging between 4.59‰ (±0.29 (2σ)) and 7.16‰ (±0.29 (2σ)) (Table A1, Appendix).

4.2. Hafnium isotopes

Initial $\varepsilon Hf_{(zircon)}$ values obtained for individual zircon grains from the plutonic rocks located in the Principal Cordillera, are distinctly positive and range between +7.7 (±1.0 (2σ)) and +10.8 (±0.8 (2σ)) (Fig. 4). These values lie close to the values projected for mantle-derived melts (i.e., new crust (NC) (Dhuime et al., 2011)), and yield hafnium model ages (T(NC)) ranging between 190 and 416 Ma (Fig. 5 and Table A1, Appendix). With the exception of the Paleocene (61.9 Ma) sample of the Los Elquinos Formation, which has $\varepsilon Hf_{T(zircon)}$ values within the range of values obtained for samples of similar age located in the Principal Cordillera (Fig. 4), the initial $\varepsilon Hf_{(zircon)}$ values of the Late Eocene (35.6 Ma) – Late Miocene (6.2 Ma) volcanic rocks present in the Frontal Cordillera range between −3.4 (±0.9 (2σ)) and +4.8 (±1.0 (2σ)), with the lowest values obtained for the youngest sample (DI095, Vacas Heladas Ignimbrites) (Fig. 4). The initial $\varepsilon Hf_{(zircon)}$ values produced for individual zircon grains from the Precordillera are generally lower than those obtained for the Principal and Fontal Cordillera and range between −3.9 (±0.6 (2σ)) and +4.1 (±0.8 (2σ)) (Figs. 4 and 5). The initial $\varepsilon Hf_{(zircon)}$ values obtained from sample PC14, the most easterly sample of the Tilito Formation (23.6 Ma), lie within this range and are lower than the $\varepsilon Hf_{T(zircon)}$ values obtained for other samples of the Tilito Formation located in the Frontal Cordillera (Fig. 4). Analyses of zircons obtained from plutonic and volcanic rocks comprising the Late Palaeozoic to Early Mesozoic basement produced initial $\varepsilon Hf_{(zircon)}$ values ranging between −2.2 (±1.0 (2σ)) and +3.0 (±1.0 (2σ)) (Fig. 5 and Table A1 of the Appendix). No correlation is observed between the initial $\varepsilon Hf_{(zircon)}$ values and the whole rock SiO_2 content (Fig. 3b).

4.3. Inherited, xenocrystic zircon cores

Devonian to Cretaceous inherited zircon cores, with $^{206}Pb/^{238}U$ ages ranging between 138.1 ± 5.2 Ma and 388.1 ± 10.5 Ma, were obtained from Late Eocene to Late Miocene plutonic and volcanic rocks from the Frontal Cordillera and Precordillera (Fig. 4). These inherited cores produced varied $\delta^{18}O_{(zircon)}$ values ranging between 4.70‰

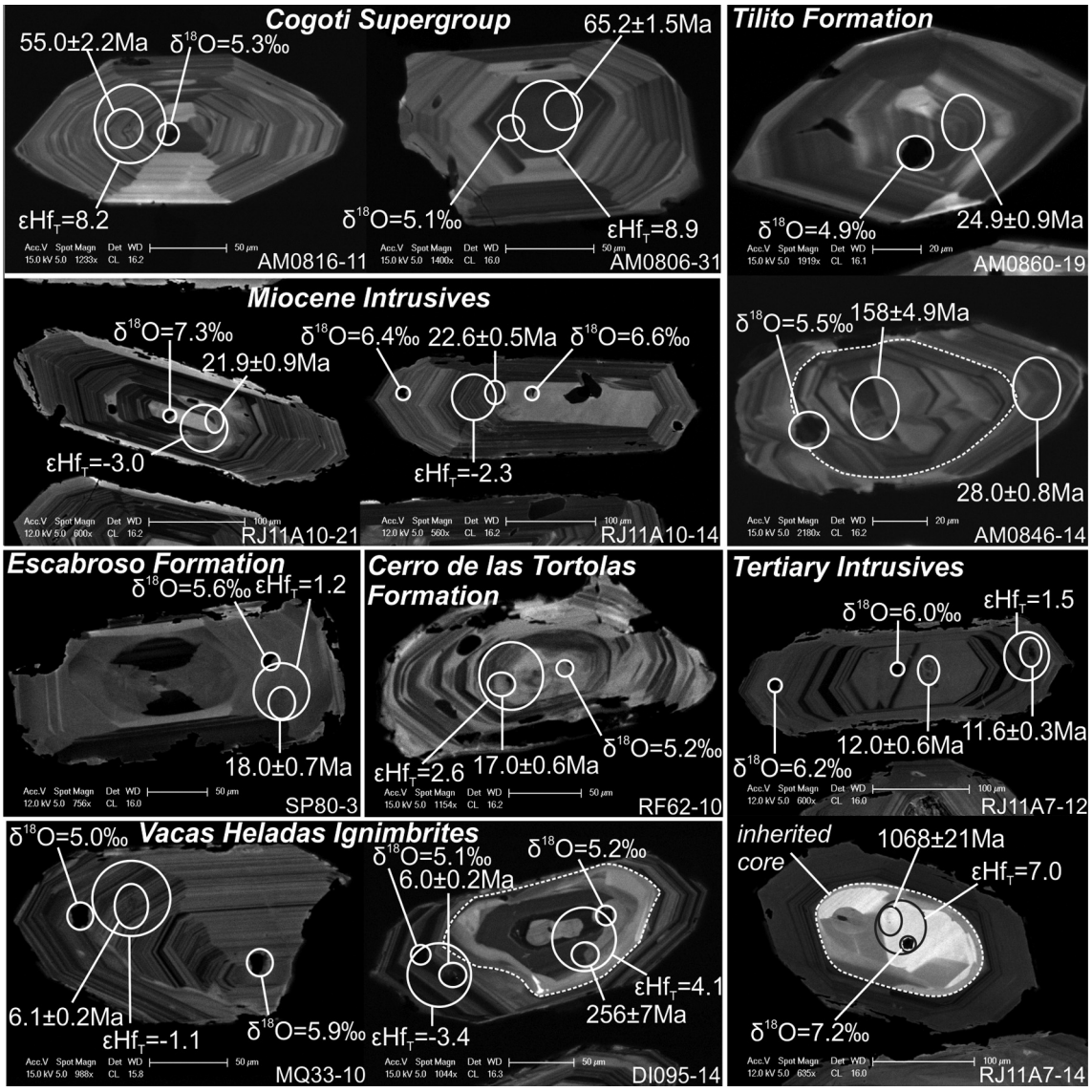

Fig. 2. Cathodoluminescence (CL) images of select zircon grains highlighting the presence of inherited cores (outlined), internal growth zoning, and the locations of *in-situ* isotopic analysis. The relative areas analysed by the different techniques (SIMS and LA-MC-ICPMS) are also indicated. The oxygen isotope ratios are expressed in $\delta^{18}O$ notation (‰) relative to VSMOW and the hafnium isotope values are expressed as initial εHf values (calculated using the $^{206}Pb/^{238}U$ age obtained by SIMS). The U–Pb ages are presented as $^{206}Pb/^{238}U$ ages for the individual zircon grains and the errors are quoted at the 2σ level.

(±0.36 (2σ)) and 9.78‰ (±0.29‰ (2σ)) and initial $\varepsilon Hf_{(zircon)}$ values ranging between −4.3 (±1.6 (2σ)) and +4.5 (±0.8 (2σ)) (Fig. 5 and Table A1, of the Appendix). These values are more varied than those obtained for zircons from samples of the Late Palaeozoic – Early Mesozoic basement (Fig. 5). Mesoproterozoic inherited cores, with $^{206}Pb/^{238}U$ ages ranging between 1249.4 ± 21.9 Ma and 1039.6 ± 29.0 Ma, were obtained from Late Miocene dacites and trachydacites (the Tertiary Intrusives) present in the Precordillera (Fig. 4). Oxygen isotope values ranging between 6.05‰ (±0.27 (2σ)) and 7.23‰ (±0.22 (2σ)) and initial $\varepsilon Hf_{(zircon)}$ values of between +7.0 (±0.6 (2σ)) and +8.4 (±0.9 (2σ)) were obtained for these inherited cores (Fig. 5 and Table A1, of the Appendix). These initial $\varepsilon Hf_{(zircon)}$ values lie close to the projected values for mantle-derived melts (i.e., new crust (NC) (Dhuime et al., 2011)) and the corresponding hafnium model ages (T(NC)) range between 1391 and 1200 Ma (Fig. 5).

5. DISCUSSION

5.1. Temporal and spatial variations in isotopic compositions

The isotopic compositions of zircons, and the occurrence and age of inherited, xenocrystic zircon cores, vary as a function of sample age and across-arc position (i.e., location in the Chilean Principal Cordillera (most westerly), Frontal Cordillera or Argentinean Precordillera (most

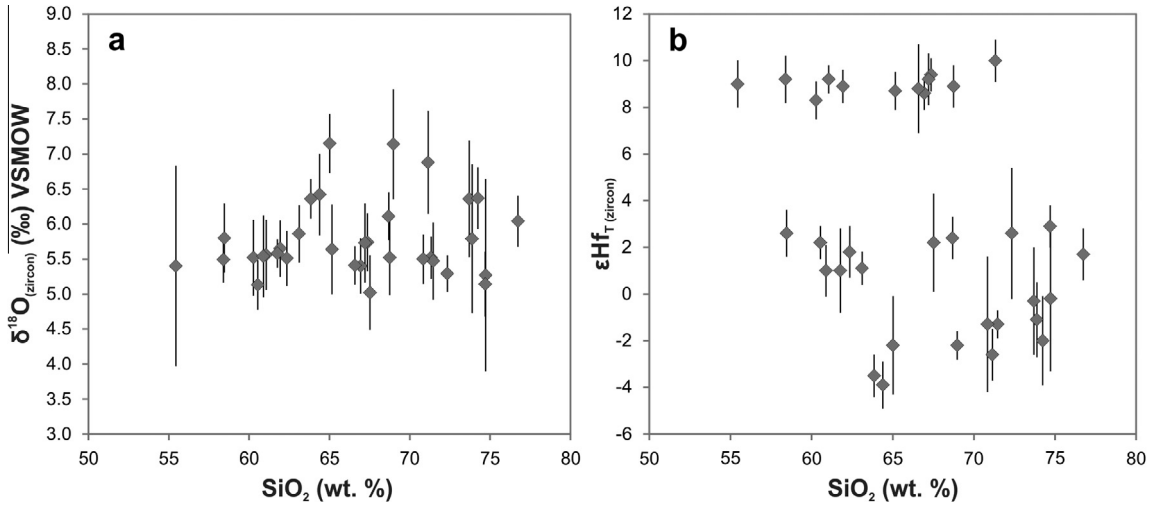

Fig. 3. Plots of (a) average $\delta^{18}O_{(zircon)}$ and (b) average $\varepsilon Hf_{T(zircon)}$ values for individual samples plotted against whole rock SiO_2 (wt.%). In samples where there is evidence for the inheritance of xenocrystic zircon cores/grains, only O and Hf isotope analyses from un-inherited cores/grains with corresponding U–Pb ages, have been used to calculate the sample averages. The error bars represent 2σ values.

easterly)), as shown in Fig. 4. Due to the eastward migration of the volcanic arc in the Pampean flat-slab segment, during the Cenozoic, the across arc position and sample age are also related.

5.2. Late Cretaceous – Eocene mantle derived melts

The 'mantle-like' $\delta^{18}O_{(zircon)}$ values obtained for the Late Cretaceous to Eocene granitoids located in the Principal Cordillera, combined with the distinctly positive, initial $\varepsilon Hf_{(zircon)}$ values, which lie close to the values projected for mantle-derived melts (Figs. 4 and 5), suggests the Late Cretaceous to Eocene arc magmas experienced very little contamination from significantly older, upper continental crust, either in the melt source region or via crustal assimilation. This interpretation is consistent with the low strontium isotope values (initial $^{87}Sr/^{86}Sr$ ratios of between 0.7035 and 0.7045) obtained for these granitoid belts (Parada et al., 1988; Parada, 1990). The absence of any significantly older, xenocrystic zircon cores (Fig. 4) provides further evidence to indicate limited interaction of these arc magmas with old continental crust. During this time interval the southern Central Andean margin is thought to have been more extensional due to the highly oblique angle of convergence between the Farallon and South American plates and low rates of convergence (e.g., Pardo Casas and Molnar, 1987; Charrier et al., 2007). Therefore, a more limited interaction between the ascending mantle-derived melts and the overlying Andean crust might be expected in comparison to later in the Cenozoic, when the continental crust became thicker due to increased compression (Kay et al., 1991).

Devonian to Triassic hafnium models ages were obtained for zircons from the Late Cretaceous – Eocene magmatic belts (Fig. 5). During this time interval the western margin of South America was located along the western margin of Gondwana and formed part of the Gondwanan magmatic arc (e.g., Kay et al., 1989; Charrier et al., 2007). On the basis of the Hf model ages, combined with the oxygen and hafnium isotope data, and whole rock geochemistry (Jones, 2014), it is suggested that the Late Cretaceous to Eocene arc magmas were derived from the asthenospheric mantle wedge with a very minor addition from Paleozoic – Early Mesozoic crust. This crustal addition could be derived from the Gondwanan magmatic arc, either due to subduction erosion or the subduction of terrigenous sediment from the arc, and/or a lower crustal reservoir which separated from the mantle during the Gondwanan tectonic cycle. An addition of older crustal material is required to account for initial $\varepsilon Hf_{(zircon)}$ values which are slightly lower (i.e., less radiogenic) than those expected for melts derived directly from the mantle (Fig. 5). Sediments have high $\delta^{18}O$ values, reflecting low temperature processes, and therefore the addition of sediment to the melt source region might be expected to raise the $\delta^{18}O_{(zircon)}$ values. Bulk mixing models suggest that a maximum addition of 4% Late Paleozoic – Early Mesozoic sediments, derived from the Andean arc, to the source of the Late Cretaceous to Eocene arc magmas could account for their initial $\varepsilon Hf_{(zircon)}$ values, whilst retaining 'mantle-like' $\delta^{18}O_{(zircon)}$ values (Fig. 6). A lower crustal reservoir which separated from the mantle during the Gondwanan tectonic cycle is also likely to have 'mantle-like' $\delta^{18}O$ values and therefore a much greater addition from such a reservoir could account for the isotopic composition of the Late Cretaceous to Eocene arc magmas. Whichever mechanism is responsible, the evidence presented by this study suggests that during the early stages of Andean-type subduction (Late Cretaceous – Eocene) there was a sustained period (~35 Ma) of upper crustal growth, with extensive magmatic belts formed from melts derived from the mantle with little recycling of pre-existing crustal material.

5.3. Controls on Late Eocene – Late Miocene isotopic variability

The contamination of arc magmas with older crustal material can occur either during magma ascent through the crust via crustal assimilation or via the subduction of

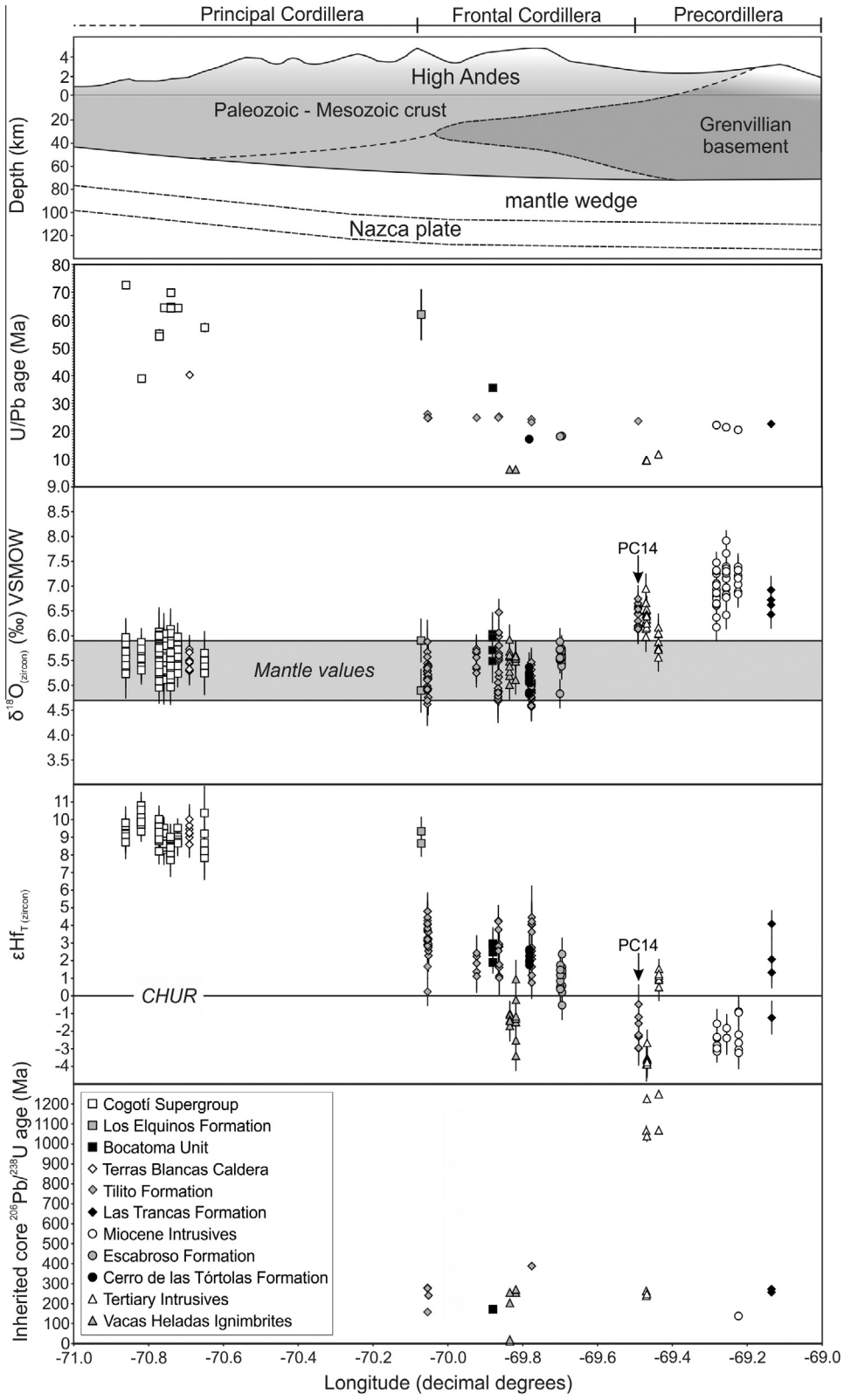

Fig. 4. Across arc variations in U–Pb crystallisation ages, $\delta^{18}O_{(zircon)}$, $\varepsilon Hf_{T(zircon)}$ (of rims or zircons without inherited cores) and inherited core $^{206}Pb/^{238}U$ ages. Error bars represent 2σ values. The isotopic data is displayed relative to a schematic cross section of the modern day Andean margin at 30° S showing the extent of the different basement terranes (Ramos et al., 2002; Gilbert et al., 2006; Heit et al., 2008). The locations of the Principal Cordillera, Frontal Cordillera, Precordillera and the Chile/Argentina border are also shown. Full results are presented in Table A1 of the Appendix.

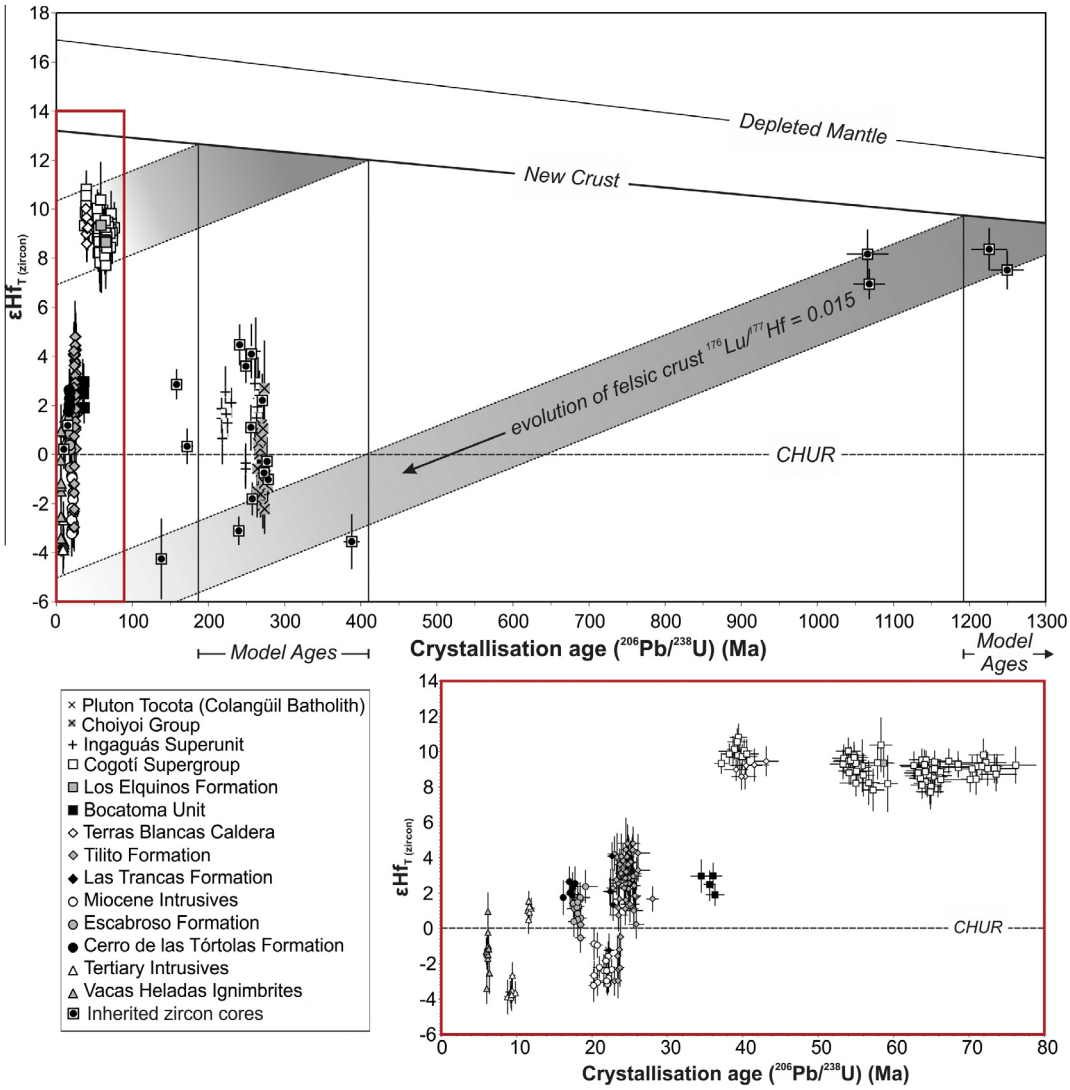

Fig. 5. Initial $\varepsilon Hf_{(zircon)}$ values plotted against crystallisation ages ($^{206}Pb/^{238}U$) (Ma) for all zircon grains and inherited cores. The data highlighted in the red box is expanded to the bottom right. Depleted mantle (DM) and new crust (NC) evolution lines are shown along with model ages for the Late Cretaceous – Eocene samples and the Proterozoic inherited cores from the Tertiary Intrusives. The initial $\varepsilon Hf_{(zircon)}$ values are presented relative to present day chondritic values (CHUR) (Bouvier et al., 2008). Error bars represent 2σ values. (For interpretation of the references to colour in this figure legend, the reader is referred to the web version of this article.)

upper crustal material (including that derived from subduction erosion) to depth. If the melt source was being contaminated, little intra- and inter-grain variation in isotopic values for samples of similar ages/from the same formations might be expected, compared to the variation which might be generated by a crystallising magma progressively assimilating continental crust (e.g., as demonstrated by core to rim changes). Temporal variations in $\delta^{18}O_{(zircon)}$ and $\varepsilon Hf_{(zircon)}$ values might also be anticipated, reflecting the subduction of different amounts of sediment and/or continental crust derived from subduction erosion, over time. Subduction erosion has been identified as an episodic process along the Central Andean margin (Kay et al., 2005; Stern, 2011), and the JFR is thought to have acted as a barrier to the transport of sediments into the trench from farther south (e.g., Bangs and Cande, 1997), after its intersection with the margin at ~20 Ma (Yañez et al., 2001, 2002). These changing dynamics might be expected to have affected the composition of the melt source region over time, by either starving or adding sediment/crustal material to the mantle wedge.

However, the variability in $\delta^{18}O_{(zircon)}$ and $\varepsilon Hf_{(zircon)}$ values obtained for Late Eocene to Late Miocene arc magmatic rocks appears to be related to geographic position relative to the Chilean margin, rather than sample age (Fig. 4). For example, sample PC14 (23.6 Ma) is contemporaneous with the Tilito Formation (Late Oligocene) and is located close to the boundary with the Precordillera. It displays distinctly different $\delta^{18}O_{(zircon)}$ and $\varepsilon Hf_{T(zircon)}$ values compared to samples of the Tilito Formation and of the same age located in the Frontal Cordillera (Fig. 4). Furthermore, the youngest samples (Vacas Heladas Ignimbrites), are located in the High Andes of the Frontal Cordillera and have $\delta^{18}O_{(zircon)}$ values which lie within the range of values obtained for other, older samples present in the Frontal Cordillera

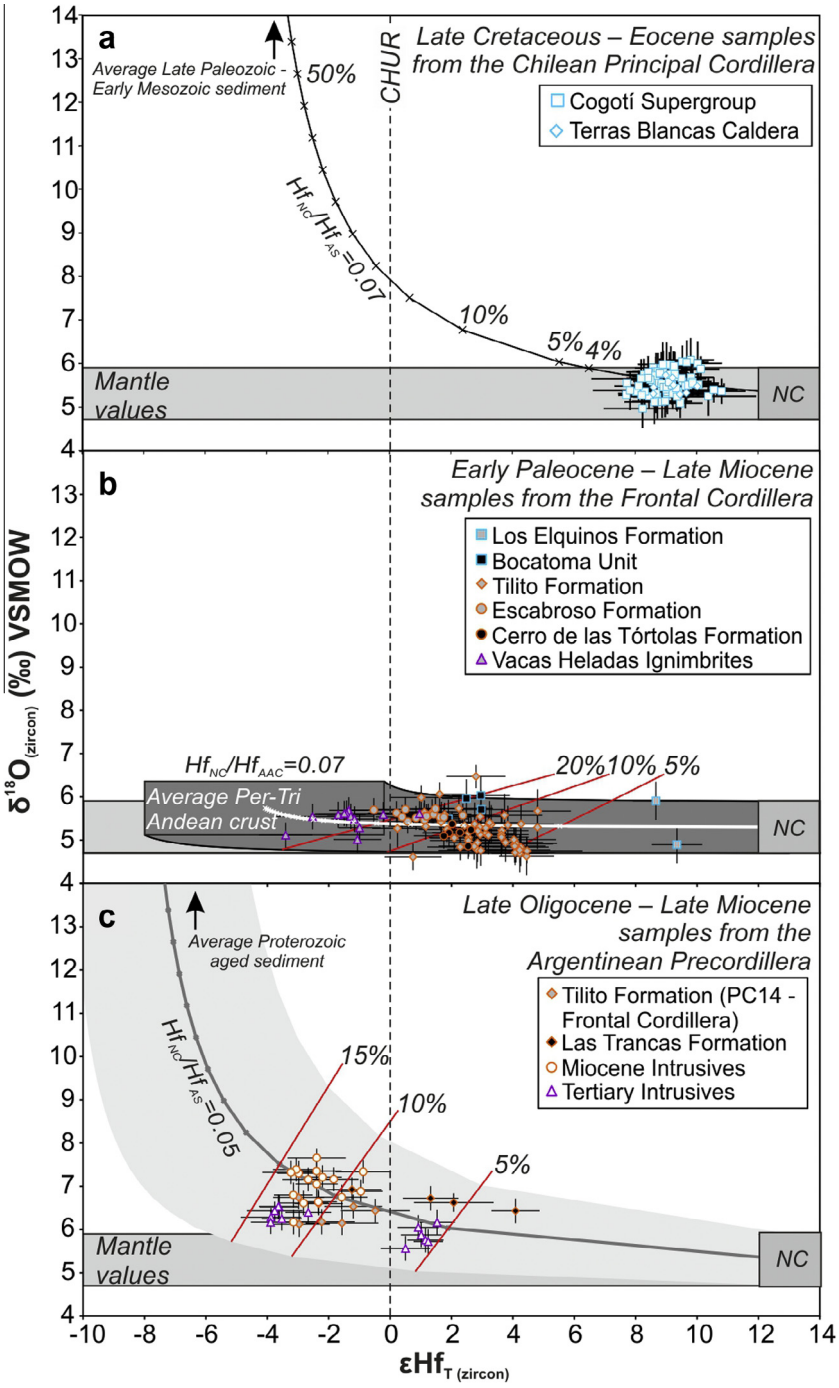

Fig. 6. Initial $\varepsilon Hf_{(zircon)}$ plotted against the corresponding $\delta^{18}O_{(zircon)}$ for (a) Late Cretaceous – Eocene samples from the Chilean Principal Cordillera, (b) Early Paleocene – Late Miocene samples from the Frontal Cordillera and (c) Late Oligocene – Late Miocene samples from the Argentinean Precordillera. A bulk mixing line between mantle-derived melts (i.e., NC (Dhuime et al., 2011)) and average Late Paleozoic – Early Mesozoic sediments is shown in a. Bulk mixing between mantle-derived melts and the Permian – Triassic basement (using a Hf_{NC}/Hf_{ACC} of 0.07) is shown to generate the observed isotopic variability in the Early Paleocene – Late Miocene samples from the Frontal Cordillera (b). Up to 15% bulk mixing between mantle-derived melts and average sediment (AS) (Savin and Epstein, 1970; Plank and Langmuir, 1998) (using a Hf_{NC}/Hf_{AS} of 0.05) explains the isotopic variability observed in the Late Oligocene – Late Miocene samples from the Argentinean Precordillera (c). Average sediment values are used to represent the basement present in the Precordillera which is suggested to be of Grenville-age and to have a sedimentary component (i.e., high $\delta^{18}O$ values) (e.g., Kay et al., 1996; Thomas and Astini, 2003). The shaded areas represent mixing between mantle-derived melts and the upper and lower values. Error bars represent 2σ values.

(Fig. 4). Intra- and inter-grain variability, particularly in $\varepsilon Hf_{(zircon)}$ values (Fig. 4), is also displayed in a number of Late Eocene – Late Miocene samples, which suggests the isotopic composition of the magma was evolving during zircon

crystallisation and was not solely determined in the melt source region.

The basement underlying the Frontal Cordillera is composed of highly deformed Paleozoic sediments which have been intruded and covered by extensive Late Palaeozoic – Early Mesozoic plutons and volcanic rocks (e.g., Kay et al., 1989). The initial $\varepsilon Hf_{(zircon)}$ values obtained for the Late Eocene to Late Miocene volcanic rocks present in the Frontal Cordillera are significantly lower (i.e., less radiogenic), than those expected for a primary melt derived from the mantle wedge (i.e., new crust (NC)) (Fig. 5), suggesting the involvement of an older, less-radiogenic crustal component. The assimilation of Paleozoic sediments by Late Eocene to Late Miocene arc magmas would result in elevated $\delta^{18}O_{(zircon)}$ values relative to the mantle. However, the majority of $\delta^{18}O_{(zircon)}$ values obtained for the Late Eocene to Late Miocene samples from the Frontal Cordillera are 'mantle-like', suggesting the contaminant must have close to 'mantle-like' $\delta^{18}O$ values which have not been affected by low temperature interaction with the hydrosphere at the Earth's surface. Analyses of zircons from Permian – Triassic plutonic and volcanic rocks present in the Frontal Cordillera, sampled as part of this study, yielded average $\delta^{18}O$ values ranging between 5.1‰ (±0.4‰, $n = 10$) and 6.4‰ (±0.9‰, $n = 12$) (Table A2). Bulk mixing models using the average $\delta^{18}O_{(zircon)}$ values obtained for the Permian – Triassic basement samples and the projected Permian – Triassic $\varepsilon Hf_{(zircon)}$ values (Fig. 5), suggests mixing of typically <20% of this crust with new mantle-derived melts (i.e., new crust (NC) (Dhuime et al., 2011)) can produce the modest changes $\delta^{18}O$, but more marked Hf isotopic variability observed in the Late Eocene to Late Miocene samples from the Frontal Cordillera (Fig. 6). The presence of primarily Permian – Triassic inherited zircon cores in these samples (Fig. 4) supports the assimilation of continental crust of this age.

The Late Oligocene – Late Miocene granitoids, andesites and rhyolites, located in the Precordillera of Argentina have higher than 'mantle-like' $\delta^{18}O_{(zircon)}$ values and un-radiogenic values of $\varepsilon Hf_{T(zircon)}$ (Figs. 4 and 5), which are quite distinct from the values obtained in the Principal and Frontal Cordillera. This suggests the interaction of these arc magmas with an ancient crustal reservoir (therefore with low εHf_T values) which has experienced low temperature interaction with the near surface, accounting for the elevated $\delta^{18}O$ values. Although no crystalline basement is exposed in the Precordillera, evidence from high-grade metamorphic, xenoliths present in the Miocene volcanic rocks indicates a Grenville-aged basement (Abbruzzi et al., 1993; Kay et al., 1996). It has been suggested that this basement forms part of a rifted fragment of Laurentian crust and passive margin cover which was accreted onto the margin of Gondwana during the Ordovician (e.g., Kay et al., 1996; Thomas and Astini, 2003). Convincing evidence for the contamination of the Late Oligocene – Late Miocene magmas with this Grenville-aged crust is provided by the presence of inherited Proterozoic cores in a number of the samples present in the Precordillera (Fig. 4). This contamination must have happened via crustal assimilation, rather than the recycling of sediments through the subduction zone, as Proterozoic crust is not exposed at the surface in the main Andean Cordillera and therefore is unlikely to have been eroded and transported into the Chilean trench.

A Grenville-aged basement is likely to have unradiogenic, negative εHf values, as shown by projecting the $\varepsilon Hf_{(zircon)}$ values obtained for the Proterozoic cores to the Cenozoic (Fig. 5), and high $\delta^{18}O$ values reflecting a sedimentary origin. Bulk mixing suggests that contamination of mantle-derived melts with up to 15% Proterozoic aged, sedimentary crust can account for the observed isotopic array displayed in zircons from the Late Oligocene – Late Miocene arc rocks of the Argentinian Precordillera (Fig. 6). This corroborates the work of Kay and Abbruzzi (1996), who suggest that mixing between melts derived from the mantle wedge and a Grenville-aged basement accounts for the distinct geochemistry of the Miocene arc magmatic rocks present in the Argentinean Precordillera. The presence of inherited cores of Permian to Cretaceous age in these Late Oligocene – Late Miocene arc rocks from the westernmost extent of the Precordillera (Fig. 4) suggests that the mantle-derived melts also assimilated Late Paleozoic – Mesozoic crust en route to the surface. Hence the O and Hf isotopic values are more likely to reflect three way mixing processes between mantle-derived melts, a Grenville-aged basement and Late Paleozoic – Mesozoic Andean crust.

The lower $\varepsilon Hf_{T(zircon)}$ values obtained for the youngest volcanic arc samples in the study area, the Vacas Heladas Ignimbrites (~6 Ma) located in the Frontal Cordillera, suggests that these arc magmas may also have interacted with an ancient portion of Andean continental crust in addition to the Late Paleozoic – Early Mesozoic crust. Structural models suggest that the Grenville-aged basement currently underthrusts the Frontal Cordillera (e.g., Ramos et al., 2004; Gilbert et al., 2006; Gans et al., 2011). Consequently the $\varepsilon Hf_{T(zircon)}$ values obtained for the Vacas Heladas Ignimbrites, which overlap those obtained for magmatic rocks present in the Precordillera, may reflect the arrival of the Grenville-aged basement under this region of the Frontal Cordillera due to increased compression and crustal shortening over the later part of the Miocene (e.g., Allmendinger et al., 1990; Kley and Monaldi, 1998; Ramos et al., 2002 and references therein). A similar argument has been made to explain evolving εNd values to the south of the study region in the southern volcanic zone (SVZ) (e.g., Muñoz et al., 2013). The development of enriched εNd values is also observed in the Pampean flat slab segment; a εNd value of −2.0 has been obtained for the Late Miocene, Vacas Heladas Ignimbrites compared to εNd values of between +1.2 and −0.1 for the Late Oligocene, Tilito Formation (Kay et al., 1991). This provides supporting evidence for the contamination of the Late Miocene arc magmas erupted in the Frontal Cordillera with the Grenville-aged basement.

During the Late Eocene to Late Miocene the products of subduction erosion and sediments present in the Chilean trench may well have entered and influenced the melt source region in the asthenospheric mantle wedge, as is suggested by high rates of subduction erosion (e.g., Stern, 2011) and exhumation along the increasingly compressional Central Andean margin (e.g., Kurtz et al., 1997; Maksaev et al.,

2003; Spikings et al., 2008). However, any effect which this subducted continental material had on the isotopic composition of the arc magmas in the melt source region appears to have been overprinted by the assimilation of the overlying crust en route to the surface, as is evidenced by the across-arc O and Hf isotopic variations which reflect the distinct basement terranes. Subduction erosion could potentially move continental crust laterally, however, this is still unlikely to generate the observed across-arc isotopic array that correlates so well with the composition of the Andean basement.

5.4. Punctuated versus steady state crustal evolution – an unbiased record

Subduction zones are considered to be sites of continental growth (e.g., Rudnick, 1995). Net growth, however, may be punctuated by periods of crustal loss due to tectonic erosion (e.g., von Huene and Scholl, 1991b; Scholl and von Huene, 2007, 2009), as is evident along the Andean margin where mass flux, and hence rates of crustal recycling have varied over time (e.g., Kay et al., 2005). It has been proposed that the Andean margin has lost ~250 km of crust over the past 150 Ma, with 30 km of trench retreat at 33° S in the last 10 Ma (Laursen et al., 2002; Clift and Hartley, 2007). If we assume an average crustal thickness of ~40 km over the study area, this equates to a loss of 2.4×10^6 km^3 of crust in the past 150 Ma. If continuous addition of crustal material to the mantle wedge occurred at a rate of 3 km/Ma as estimated at 33° S, then implicitly variable but recognizable signatures of crustal contamination should be observable. This is not the case for the samples analysed from the southern Central Andes. Intrusive rocks dated from Late Cretaceous (~73 Ma) to Eocene (~39 Ma) record a sustained period of upper crustal growth, with very limited evidence of contamination by older continental crust. From ~36 Ma to 17 Ma however there is good evidence for mixing of mantle-derived melts with Late Palaeozoic – Early Mesozoic basement. This could be the result of increased sediment flux to the trench and ultimately the mantle wedge, or as a result of increased subduction erosion of the margin. In the Late Oligocene (~23 Ma) to Late Miocene (~6 Ma) at least two types of basement that differ in age are required to generate the isotopic variability observed, i.e., a mixture of Grenville and Palaeozoic basement. As no crust of Grenville age occurs close to the margin it is indicative of crustal assimilation and recycling. This is consistent with the conclusions of Clift and Hartley (2007) that the forearc has eroded slowly since ~20 Ma and that subduction erosion is punctuated over time. Interestingly the timing of episodes of high flux do not correspond with those further north between 15 and 25° S which peaked at ~80, 40 and <10 Ma ago (DeCelles et al., 2009); suggesting considerable spatial variability in flux along the length of the margin.

Models for the growth of continental crust rely on knowing the balance between the generation of new crust and the reworking of old crust. A number of studies (e.g., Kemp et al., 2006; Belousova et al., 2010; Dhuime et al., 2012; Wang et al., 2013) have used similar techniques to those applied here to unravel the preserved sedimentary record, which is just a snap shot of the overall signal. In this study, where the spatial relationship between samples is well constrained, along and across margin variability in the zircon record is revealed. Such spatial variability could be averaged by sediment transport processes and thus be masked if only using sediments to reveal the growth of continental crust over geological time (Allègre and Rousseau, 1984).

6. CONCLUSIONS

It is evident that combining the *in-situ* analysis of the oxygen and hafnium isotopic composition of magmatic zircon, with high resolution U–Pb dating, can be used to identify the spatial contamination of arc magmas with specific portions of crust during one tectonic cycle. This has significant implications for models of continental growth, particularly in settings where the geodynamics and plate tectonics are poorly understood, for example in the early Earth, demonstrating that wide variations in $\delta^{18}O_{(zircon)}$ and $\varepsilon Hf_{(zircon)}$ values can be generated over relatively short distances (10's kms). This approach demonstrates that as the geodynamic setting of the southern Central Andean margin changed (the subducting Nazca plate shallowed, the continental crust thickened, and the position of arc magmatism migrated to the east), the Late Eocene to Late Miocene mantle-derived magmas became contaminated (via assimilation) with distinct basement domains. The age and composition of the pre-existing continental crust, which is spatially variable over the Andean Cordillera, is shown to play the dominant role (over the contamination of mantle wedge with subducting components or the products of subduction erosion) in modifying the isotopic composition of the Late Eocene to Late Miocene mantle-derived melts. In comparison to the early Cenozoic, which is shown to represent a period of upper crustal growth with little recycling of crustal material, the Late Eocene to Late Miocene is identified as representing a sustained period of crustal reworking in the southern Central Andes.

ACKNOWLEDGEMENTS

This work was funded by a NERC CASE studentship (NE/G524128/1) and the Derek and Maureen Moss Scholarship. In addition, Linda Kirstein received support from the Carnegie Trust for the Universities of Scotland. None of the funding sources were directly involved in the scientific work or the interpretation of the data. We are grateful to Benjamin Heit, Dante Scatolon and Eduardo Campos for help with fieldwork and logistics. SIMS analysis at the EIMF was supported by NERC (IMF425/1010). John Craven is thanked for his expertise and assistance in oxygen isotope analysis. We are grateful to Nicola Cayzer for guidance in SEM imaging, Chris Hayward for assistance in EPMA, and to Mike Hall and Robert McDonald for help with sample preparation.

APPENDIX A. SUPPLEMENTARY DATA

Supplementary data associated with this article can be found, in the online version, at http://dx.doi.org/10.1016/j.gca.2015.05.007.

REFERENCES

Abbruzzi J., Kay S. M. and Bickford M. E. (1993) Implications for the nature of the Precordilleran basement from the geochemistry and age of Precambrian xenoliths in Miocene volcanic rocks, San Juan province. *Actas* **3**, 331–339.

Allègre C. J. and Rousseau D. (1984) The growth of the continent through geological time studied by Nd isotope analysis of shales. *Earth Planet. Sci. Lett.* **67**, 19–34.

Allmendinger R. W., Figueroa D., Snyder D., Beer J., Mpodozis C. and Isacks B. L. (1990) Foreland shortening and crustal balancing in the Andes at 30° S latitude. *Tectonics* **9**, 789–809.

Bangs N. L. and Cande S. C. (1997) Episodic development of a convergent margin inferred from structures and processes along the southern Chile margin. *Tectonics* **16**, 489–503.

Belousova E. A., Kostitsyn Y. A., Griffin W. L., Begg G. C., O'Reilly S. Y. and Pearson N. J. (2010) The growth of the continental crust: constraints from zircon Hf-isotope data. *Lithos* **119**, 457–466.

Bissig T., Lee J. K. W., Clark A. H. and Heather K. B. (2001) The Cenozoic History of Volcanism and Hydrothermal Alteration in the Central Andean Flat-Slab Region: new 40Ar-39Ar Constraints from the El Indio-Pascua Au (-Ag, Cu) Belt, 29°20′–30°30′ S. *Int. Geol. Rev.* **43**, 312–340.

Bissig T., Clark A. H., Lee J. K. and von Quadt A. (2003) Petrogenetic and metallogenetic responses to Miocene slab flattening: new constraints from the El Indio-Pascua Au–Ag–Cu belt, Chile/Argentina. *Miner. Deposita* **38**, 844–862.

Bouvier A., Vervoort J. D. and Patchett P. J. (2008) The Lu-Hf and Sm-Nd isotopic composition of CHUR: constraints from unequilibrated chondrites and implications for the bulk composition of terrestrial planets. *Earth Planet. Sci. Lett.* **273**, 48–57.

Cardó R. and Díaz I. N. (1999). Hoja Geológica 3169-I, Rodeo, provincias de San Juan. Instituto de Geología y Recursos Minerales, Servicio Geológico Minero Argentino, Buenos Aires.

Cardó R., Díaz I. N., Limarino C. O., Litvak V. D., Poma S. and Santamaria G. (2007) Hoja Geológica 2969-III, Malimán, provincias de San Juan y La Rioja, Boletín 320 ed. Instituto de Geología y Recursos Minerales, Servicio Geológico Minero Argentino, Buenos Aires.

Charchaflié D., Tosdal R. M. and Mortensen J. K. (2007) Geologic framework of the Veladero high-sulfidation epithermal deposit area, Cordillera Frontal, Argentina. *Econ. Geol.* **102**, 171–192.

Charrier R., Pinto L. and Rodríguez M. P. (2007) Tectonostratigraphic evolution of the Andean Orogen in Chile. In *The Geology of Chile* (eds. T. Moreno and W. Gibbons). The Geological Society, London, pp. 21–114.

Clayton R. N., O'Neil J. R. and Mayeda T. K. (1972) Oxygen isotope exchange between quartz and water. *J. Geophys. Res.* **77**, 3057–3067.

Clift P. D. and Hartley A. J. (2007) Slow rates of subduction erosion and coastal underplating along the Andean margin of Chile and Peru. *Geology* **35**, 503–506.

Davidson J. P., Harmon R. S. and Wörner G. (1991) The source of central Andean magmas; Some considerations. *Geolog. Soc. Am.* **265**, 233–244, Special Papers.

DeCelles P. G., Ducea M. N., Kapp P. and Zandt G. (2009) Cyclicity in Cordilleran orogenic systems. *Nat. Geosci.* **2**, 251–257.

Dhuime B., Hawkesworth C. and Cawood P. (2011) When continents formed. *Science* **331**, 154–155.

Dhuime B., Hawkesworth C. J., Cawood P. A. and Storey C. D. (2012) A change in the geodynamics of continental growth 3 billion years ago. *Science* **335**, 1334–1336.

Eiler J. M. (2001) Oxygen isotope variations of basaltic lavas and upper mantle rocks. *Rev. Mineral. Geochem.* **43**, 319–364.

Emparan C. and Pineda G. (1999) Area Condoriaco-Rivadavia, Región de Coquimbo. Servicio Nacional de Geologia y Mineria, Mapas Geológicos, Santiago.

Gans C. R., Beck S. L., Zandt G., Gilbert H., Alvarado P., Anderson M. and Linkimer L. (2011) Continental and oceanic crustal structure of the Pampean flat slab region, western Argentina, using receiver function analysis: new high-resolution results. *Geophys. J. Int.* **186**, 45–58.

Gilbert H., Beck S. and Zandt G. (2006) Lithospheric and upper mantle structure of central Chile and Argentina. *Geophys. J. Int.* **165**, 383–398.

Gill J. B. (1981) *Orogenic Andesites and Plate Tectonics*. Springer-Verlag, New York.

Goss A. R., Kay S. M. and Mpodozis C. (2013) Andean Adakite-like high-Mg Andesites on the Northern Margin of the Chilean-Pampean Flat-slab (27–28· 5° S) associated with Frontal Arc Migration and Fore-arc Subduction Erosion. *J. Petrol.* **54**, 2193–2234.

Haschke M., Siebel W., Günther A. and Scheuber E. (2002) Repeated crustal thickening and recycling during the Andean orogeny in north Chile (21°–26° S). *J. Geophys. Res. Solid Earth* **107**, ECV 6-1-ECV 6–18.

Hawkesworth C. J. and Kemp A. I. S. (2006) Using hafnium and oxygen isotopes in zircons to unravel the record of crustal evolution. *Chem. Geol.* **226**, 144–162.

Heit B., Yuan X., Bianchi M., Sodoudi F. and Kind R. (2008) Crustal thickness estimation beneath the southern central Andes at 30° S and 36° S from S wave receiver function analysis. *Geophys. J. Int.*.

Jarvis A., Reuter H. I., Nelson A. and Guevara E. (2008) Hole-filled SRTM for the globe Version 4, Available from the CGIAR-CSI SRTM 90m Database.

Jones R. E. (2014) *Subduction zone processes and continental crust formation in the southern Central Andes: Insights from geochemistry and geochronology*. School of GeoSciences, The University of Edinburgh, Edinburgh.

Jones R. E., De Hoog J. C. M., Kirstein L. A., Kasemann S. A., Hinton R., Elliott T. and Litvak V. D. (2014) Temporal variations in the influence of the subducting slab on Central Andean arc magmas: evidence from boron isotope systematics. *Earth Planet. Sci. Lett.* **408**, 390–401.

José Frutos J., Paula Cornejo P., Tomlinson A., Arturo Hauser Y., Carlos Portigliati N., Aníbal Gajardo C., Estanislao Godoy P. -B., Ernesto Pérez D. A. and Renate Wall Z. (2004) Mapa Geológico de Chile: versión digital, Carta Geológica de Chile, Serie Geología Básica, CD-ROM, versión 1.0, 2004 ed. Servicio Nacional de Geología y Minería (SERNAGEOMIN), Santiago.

Kay S. M. and Abbruzzi J. M. (1996) Magmatic evidence for Neogene lithospheric evolution of the central Andean "flat slab" between 30° S and 32° S. *Tectonophysics* **259**, 15–28.

Kay S. M. and Mpodozis C. (2001) Central Andean ore deposits linked to evolving shallow subduction systems and thickening crust. *GSA Today* **11**, 4–9.

Kay S. M. and Mpodozis C. (2002) Magmatism as a probe to the Neogene shallowing of the Nazca plate beneath the modern Chilean flat slab. *J. South Am. Earth Sci.* **15**, 39–57.

Kay S. M., Orrell S. and Abbruzzi J. (1996) Zircon and whole rock Nd-Pb isotopic evidence for a Grenville age and a Laurentian origin for the basement of the Precordillera in Argentina. *J. Geol.*, 637–648.

Kay S.M., Mpodozis C. and Coira B. (1999). Neogene magmatism, tectonism, and mineral deposits of the Central Andes (22 to 33 S latitude). In *Geology and Ore Deposits of the Central Andes*

(ed. B.J. Skinner). Society of Economic Geologists, Special Publication 7, pp. 27–59.

Kay S. M., Godoy E. and Kurtz A. (2005) Episodic arc migration, crustal thickening, subduction erosion, and magmatism in the south-central Andes. *Geol. Soc. Am. Bull.* **117**, 67–88.

Kay S. M., Maksaev V., Moscoso R., Mpodozis C. and Nasi C. (1987) Probing the evolving Andean lithosphere; Mid – Late Tertiary magmatism in Chile (29°–30°30′ S) over the modern zone of subhorizontal subduction. *J. Geophys. Res.* **92**, 6173–6189.

Kay S. M., Ramos V. A., Mpodozis C. and Sruoga P. (1989) Late Paleozoic to Jurassic silicic magmatism at the Gondwana margin: analogy to the Middle Proterozoic in North America? *Geology* **17**, 324–328.

Kay S. M., Mpodozis C., Ramos V. A. and Munizaga F. (1991) Magma source variations for mid-late Tertiary magmatic rocks associated with a shallowing subduction zone and the thickening crust in the Central Andes (28–33° S). *Spec. Pap. Geol. Soc. Am. Bull.* **265**, 113–137.

Kemp A. I. S., Hawkesworth C. J., Paterson B. A. and Kinny P. D. (2006) Episodic growth of the Gondwana supercontinent from hafnium and oxygen isotopes in zircon. *Nature* **439**, 580–583.

Kemp A. I. S., Hawkesworth C. J., Foster G. L., Paterson B. A., Woodhead J. D., Hergt J. M., Gray C. M. and Whitehouse M. J. (2007) Magmatic and crustal differentiation history of granitic rocks from Hf-O isotopes in zircon. *Science* **315**, 980–983.

Kinny P. D. and Maas R. (2003) Lu–Hf and Sm–Nd isotope systems in zircon. In *Zircon: Reviews in Mineralogy and Geochemistry* (eds. J. M. Hanchar and P. W. O. Hoskin). Mineralogical Society of America/Geochemical Society, Washington DC, pp. 327–339.

Kley J. and Monaldi C. R. (1998) Tectonic shortening and crustal thickness in the Central Andes: how good is the correlation? *Geology* **26**, 723–726.

Kurtz A. C., Kay S. M., Charrier R. and Farrar E. (1997) Geochronology of Miocene plutons and exhumation history of the El Teniente region, Central Chile (34–35° 8). *Andean Geol.* **24**, 75–90.

Laursen J., Scholl D. W. and von Huene R. (2002) Neotectonic deformation of the central Chile margin: deepwater forearc basin formation in response to hot spot ridge and seamount subduction. *Tectonics* **21**, 1038.

Litvak V. D., Poma S. and Kay S. M. (2007) Paleogene and Neogene magmatism in the Valle del Cura region: new perspective on the evolution of the Pampean flat slab, San Juan province, Argentina. *J. South Am. Earth Sci.* **24**, 117–137.

Lonsdale P. (2005) Creation of the Cocos and Nazca plates by fission of the Farallon plate. *Tectonophysics* **404**, 237–264.

Maksaev V., Moscoso R., Mpodozis C. and Nasi C. (1984) Las unidades volcánicas y plutónicas del Cenozoico superior en la alta cordillera del Norte Chico (29–31 S): Geología, alteración hidrotermal y mineralización. *Rev. Geol. Chile*, 11–51.

Maksaev V., Zentilli M., Munizaga F. and Charrier R. (2003). Denudación/alzamiento del Mioceno Superior-Plioceno Inferior de la Cordillera de Chile Central (33°–35° S) inferida por dataciones por trazas de fisión en apatito de plutones miocenos, Congreso Geológico Chileno.

Marfil S. and Maiza P. (2012) Geochemistry of hydrothermal alteration in volcanic rocks. In *Geochemistry – Earth's System Processes* (ed. D. Panagiotaras).

McCarthy T. S. and Hasty R. A. (1976) Trace element distribution patterns and their relationship to the crystallization of granitic melts. *Geochim. Cosmochim. Acta* **40**, 1351–1358.

Mpodozis C. and Cornejo P. P. (1988) Hoja Pisco Elqui, Region de Coquimbo. In *Carta Geologica de Chile* (eds. C. Mpodozis, J. Davidson and S. Rivano). Servicio Nacional de Geología y Minería (SERNAGEOMIN), Santiago.

Muñoz M., Farías M., Charrier R., Fanning C. M., Polvé M. and Deckart K. (2013) Isotopic shifts in the Cenozoic Andean arc of central Chile: records of an evolving basement throughout cordilleran arc mountain building. *Geology* **41**, 931–934.

Nasi C., Moscoso R. and Maksaev V. (1990) Hoja Guanta Regiones de Atacama y Coquimbo. In *Carta Geologica de Chile* (eds. C. Mpodozis, J. Davidson and S. Rivano). Servicio Nacional de Geología y Minería (SERNAGEOMIN), Santiago.

Parada M. A. (1990) Granitoid plutonism in central Chile and its geodynamic implications; a review. In *Plutonism from Antarctica to Alaska* (eds. S. M. Kay and C. W. Rapela). The Geological Society of America, Boulder, Colorado.

Parada M. A., Rivano S., Sepulveda P., Herve M., Herve F., Puig A., Munizaga F., Brook M., Pankhurst R. and Snelling N. (1988) Mesozoic and Cenozoic plutonic development in the Andes of central Chile (30°30′–32°30′ S). *J. South Am. Earth Sci.* **1**, 249–260.

Pardo Casas F. and Molnar P. (1987) Relative motion of the Nazca (Farallón) and South America plates since Late Cretaceous time. *Tectonics* **6**, 233–248.

Patchett J. P., Kouvo O., Hedge C. and Tatsumoto M. (1982) Evolution of continental crust and mantle heterogeneity: evidence from Hf isotopes. *Contrib. Mineral. Petrol.* **78**, 279–297.

Peck W. H., Valley J. W. and Graham C. M. (2003) Slow oxygen diffusion rates in igneous zircons from metamorphic rocks. *Am. Mineral.* **88**, 1003–1014.

Pichowiak S., Buchelt M. and Damm K. (1990) Magmatic activity and tectonic setting of the early stages of the Andean cycle in northern Chile. In: *Plutonism from Antarctica to Alaska* (eds, S.M. Kay, C.W. Rapela) Geological Society of America, Special Paper 241, pp. 127–144.

Pilger R. H. (1981) Plate reconstructions, aseismic ridges, and low angle subduction beneath the Andes. *Geol. Soc. Am. Bull.* **92**, 448–456.

Pilger R. H. (1984) Cenozoic plate kinematics, subduction and magmatism: South American Andes. *J. Geol. Soc. Lond.* **141**, 793–802.

Pineda G. and Emparan C. (2006) Geología del área Vicuña-Pichasca, Región de Coquimbo, Carta Geológica de Chile, Serie Geología Básica Servicio Nacional de Geología y Minería, Santiago.

Pineda G. and Calderón M. (2008) Geología del área Monte Patria-El Maqui, Región de Coquimbo, Carta Geológica de Chile, Serie Geología Básica. Servicio Nacional de Geología y Minería, Santiago.

Plank T. and Langmuir C. H. (1998) The chemical composition of subducting sediment and its consequences for the crust and mantle. *Chem. Geol.* **145**, 325–394.

Ramos V. A. (2010) The Grenville-age basement of the Andes. *J. South Am. Earth Sci.* **29**, 77–91.

Ramos V. A., Cristallini E. and Pérez D. J. (2002) The Pampean flat-slab of the Central Andes. *J. South Am. Earth Sci.* **15**, 59–78.

Ramos V. A., Jordan T. E., Allmendinger R. W., Mpodozis C., Kay S. M., Cortés J. M. and Palma M. (1986) Paleozoic terranes of the central Argentine-Chilean Andes. *Tectonics* **5**, 855–880.

Ramos V. A., Zapata T., Cristallini E. and Introcaso A. (2004) The Andean thrust system—latitudinal variations in structural styles and orogenic shortening. *Thrust Tectonics Hydrocarbon Syst.* **82**, 30–50.

Rutland R. W. R. (1971) Andean orogeny and ocean floor spreading. *Nature* **233**, 252–255.

Rudnick R. L. (1995) Making continental crust. *Nature* **378**, 573–578.

Savin S. M. and Epstein S. (1970) The oxygen and hydrogen isotope geochemistry of clay minerals. *Geochim. Cosmochim. Acta* **34**, 25–42.

Scholl D. W. and von Huene R. (2007) Crustal recycling at modern subduction zones applied to the past-issues of growth and preservation of continental basement crust, mantle geochemistry and supercontinent reconstruction. In *4-D Framework of Continental Crust* (eds. R. D. Hatcher, M. P. Carlson, J. H. McBride and J. R. M. Catalán). Geological Society of America Memoir, pp. 9–32.

Scholl D. W. and von Huene R. (2009) Implications of estimated magmatic additions and recycling losses at the subduction zones of accretionary (non-collisional) and collisional (suturing) orogens. In *Earth Accretionary Systems in Space and Time* (eds. P. A. Cawood and A. Kröner). Geological Society, London, pp. 105–125, Special Publications.

Somoza R. (1998) Updated Nazca (Farallon)–South America relative motions during the last 40My: implications for mountain building in the central Andean region. *J. South Am. Earth Sci.* **11**, 211–215.

Somoza R. and Ghidella M. E. (2012) Late Cretaceous to recent plate motions in western South America revisited. *Earth Planet. Sci. Lett.* **331–332**, 152–163.

Spikings R., Dungan M., Foeken J., Carter A., Page L. and Stuart F. (2008) Tectonic response of the central Chilean margin (35–38 S) to the collision and subduction of heterogeneous oceanic crust: a thermochronological study. *J. Geol. Soc.* **165**, 941–953.

Stern C. R. (1991) Role of subduction erosion in the generation of Andean magmas. *Geology* **19**, 78–81.

Stern C. R. (2004) Active Andean volcanism: its geologic and tectonic setting. *Rev. Geol. Chile* **31**, 161–206.

Stern C. R. (2011) Subduction erosion: rates, mechanisms, and its role in arc magmatism and the evolution of the continental crust and mantle. *Gondwana Res.* **20**, 284–308.

Thomas W. A. and Astini R. A. (2003) Ordovician accretion of the Argentine Precordillera terrane to Gondwana: a review. *J. South Am. Earth Sci.* **16**, 67–79.

Thomas W. A., Astini R. A., Mueller P. A., Gehrels G. E. and Wooden J. L. (2004) Transfer of the Argentine Precordillera terrane from Laurentia: constraints from detrital-zircon geochronology. *Geology* **32**, 965–968.

Valley J. W. (2003) Oxygen isotopes in zircon, In: *Zircons. Reviews in Mineralogy and Geochemistry, Mineralogical Society of America* (eds. J.M. Hanchar and P.W.O. Hoskin). Chantilly, Virginia. pp. 343–386.

Valley J. W., Kinny P. D., Schulze D. J. and Spicuzza M. J. (1998) Zircon megacrysts from kimberlite: oxygen isotope variability among mantle melts. *Contrib. Mineral. Petrol.* **133**, 1–11.

Von Huene R. and Scholl D. W. (1991a) Observations at convergent margins concerning sediment subduction, subduction erosion, and the growth of continental crust. *Rev. Geophys.* **29**.

von Huene R. and Scholl D. W. (1991b) Observations at convergent margins concerning sediment subduction, subduction erosion, and the growth of continental crust. *Rev. Geophys.* **29**, 279–316.

Wang L.-J., Griffin W. L., Yu J.-H. and O'Reilly S. Y. (2013) U–Pb and Lu–Hf isotopes in detrital zircon from Neoproterozoic sedimentary rocks in the northern Yangtze Block: implications for Precambrian crustal evolution. *Gondwana Res.* **23**, 1261–1272.

Yañez G. A., Ranero C. R., von Huene R. and Díaz J. (2001) Magnetic anomaly interpretation across the southern Central Andes (32–34° S): the role of the Juan Fernández Ridge in the late Tertiary evolution of the margin. *J. Geophys. Res.* **106**, 6325–6345.

Yañez G. A., Cembrano J., Pardo M., Ranero C. R. and Selles D. (2002) The Challenger–Juan Fernández–Maipo major tectonic transition of the Nazca–Andean subduction system at 33–34° S: geodynamic evidence and implications. *J. South Am. Earth Sci.* **15**, 28–38.

Associate editor: Janne Blichert-Toft